Journal of Organometallic Chemistry 694 (2009) 1848–1860

Contents lists available at ScienceDirect

Journal of Organometallic Chemistry

journal homepage: www.elsevier.com/locate/jorganchem

Electronic structures and optical properties of neutral substituted fluorene-based cyclometalated platinum(II)–acetylide complexes: A DFT exploration

Fu-Quan Bai [a], Xin Zhou [a], Bao-Hui Xia [a,b], Tao Liu [a], Jian-Po Zhang [a], Hong-Xing Zhang [a,*]

[a] State Key Laboratory of Theoretical and Computational Chemistry, Institute of Theoretical Chemistry, Jilin University, Changchun 130023, People's Republic of China
[b] College of Chemistry, Jilin University, Changchun 130023, People's Republic of China

ARTICLE INFO

Article history:
Received 11 November 2008
Received in revised form 10 January 2009
Accepted 13 January 2009
Available online 20 January 2009

Keywords:
Platinum
Acetylide
Fluorene
Optical properties
DFT
Electronic structures

ABSTRACT

We report a combinational DFT and TD-DFT study of the electronic and optical properties of several tridentate cyclometalated mononuclear [Pt(C^N^N)(C≡CR)] (**1**–**3**), [Pt(C^N^N)(C≡CRC≡CH)] (**4**), and dinuclear [Pt(C^N^N)(C≡CRC≡C)Pt(C^N^N)] (**5** (C_2 symmetry) and **5′** (C_s symmetry)) platinum(II) complexes with σ-acetylide ligand bearing fluorene substituents, where HC^N^N = 6-aryl-2,2′-bipyridine, R = fluorene-2,7-diyl **1**, **4**, **5** and **5′**, R = 9,9-dimethylfluorene-2,7-diyl **2**, R = 9,9-diethylfluorene-2,7-diyl **3**. The structural and electronic properties of the ground- and lowest triplet state and the EA and IP values of the complexes are discussed. It is found that all of the lowest-lying absorptions are categorized as the LLCT combined with the MLCT transitions. The oscillator strengths of the lowest energy absorptions get a remarkable enhancement for the dinuclear complexes **5** and **5′**compared to **1**–**4** due to the increase of electronic delocalization on the more planar molecular geometry. In general, the phosphorescent emissions of these complexes in CH_2Cl_2 are the reverse process of their lowest energy absorption transitions, except that of **4** is assigned as $^3[\pi^*-\pi]/^3$MLCT transition because of the strengthened electronic localization effect and the interaction with the solvent in the lowest triplet state. In addition, these complexes hold promise as a new kind of nonlinear optical material owing to their large static first hyperpolarizabilities (β_0). The β_0 value has increased in the dinuclear complexes in contrast to those of the mononuclear ones owing to their larger transition moment and smaller transition energy.

1. Introduction

Since the mid-1980s, the study of transition-metal σ-alkynyl complexes has been an intense area of research, because they hold a fascination for synthetic, structural, and material scientists alike [1–11]. The linear geometry of the alkynyl unit and its π-unsaturated character led to metal alkynyls becoming attractive building blocks for molecular wires and polymeric organometallic materials, which can possess interesting properties, such as optical nonlinearity, luminescence, liquid crystallinity, and electrical conductivity [12–26]. Since the applications of organic light-emitting diodes (OLEDs) were tremendously developed by Tang and Van Slyke using the metal–organic Alq_3 (q = hydroxyquinoline) as the fluorescent emitter, the design and synthesis of luminescent transition-metal σ-alkynyl complexes have received much attention [27–33].

Particularly, in recent years, there has been particular interest in platinum(II) alkynyl complexes for molecular photochemical devices manifolds due to their chemical and structural stability, greater conduction bandwidth, as well as the directional nature of the charge transfer (CT) excited states which is ideal for electron–hole creation and separation in square-planar coordination geometry [34,35]. From wide-ranging spectroscopic and magnetic studies, the alkynyl ligand is shown to occupy "strong-field" positions in the spectrochemical series. Thus, alkynyl ligands can be interpreted as good π donors and poor π acceptors. Two classes of platinum(II) σ-alkynyl frameworks have been widely reported: one includes Pt mono-alkynyl and the others consist of Pt dialkynyl with *trans*- and *cis*-modes. Aiming at enhancing the device performances and tuning the photophysical and electroluminescent properties, a vast range of platinum-containing monomers and polymers have been prepared [36–42]. Raithby and co-workers reported a series of blue-luminescent [$Pt(P^nBu_3)_2$–C≡C–X–C≡C–] (X = aromatic spacer) based polymers in the main chain in which the aromatic rings bearing extensive π-conjugation is useful to change the spectroscopic properties [43]. In contrast to hydrocarbon conjugated polymers, the triplet excited states of this kind of polymers are accessible experimentally by various optical methods. The electron-rich fluorene derivatives were recently utilized as the spacer groups, since they showed interesting and unique chemical and physical properties because of the rigid planar biphenyl unit. Furthermore, the facile substitution at the remote C-9 position in fluorene unit can improve the solubility and processability

* Corresponding author. Tel./Fax: +86 431 88498966.
E-mail address: zhanghx@mail.jlu.edu.cn (H.-X. Zhang).

0022-328X/$ - see front matter © 2009 Elsevier B.V. All rights reserved.
doi:10.1016/j.jorganchem.2009.01.020

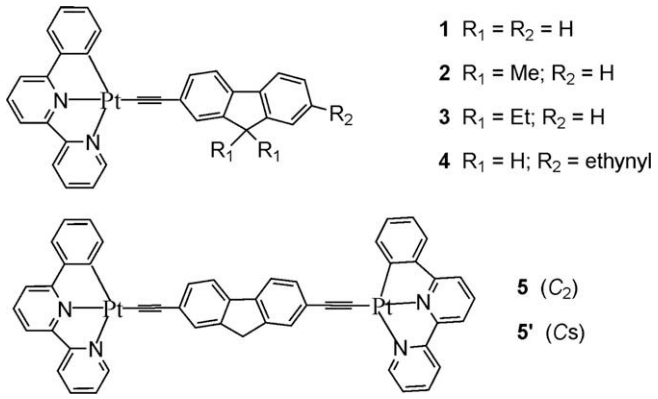

Chart 1.

of polymers without significantly increasing the steric interactions in the polymer backbone [44–47]. Wong and co-workers studied a group of soluble platinum diyne and polyyne materials consisting of fluorene linking units, and a systematic correlation was made between the effective conjugation length (or conversely, band gap) and the intersystem crossing rate in these polyynes [44,48].

The emission of the aforementioned materials was assigned to triplet intraligand (IL) charge transfer transition perturbed by some ^{3}MLCT transition [15,48]. The low-lying π^* orbitals were strongly localized or delocalized over the main chain. Many spectroscopic and theoretical investigation revealed that many multidentate cyclometalated ligands such as aromatic diimine also features low-lying π^* orbitals [49–53]. Therefore, the luminescent cyclometalated Pt(II) σ-alkynyl species are another way to design and synthesize promising materials in OLEDs as well as photoinduced charge-separation systems. In 1994, Che and co-workers reported the first diimine complexes [Pt(phen)(C≡CPh)$_2$] (phen = 1, 10-phe-

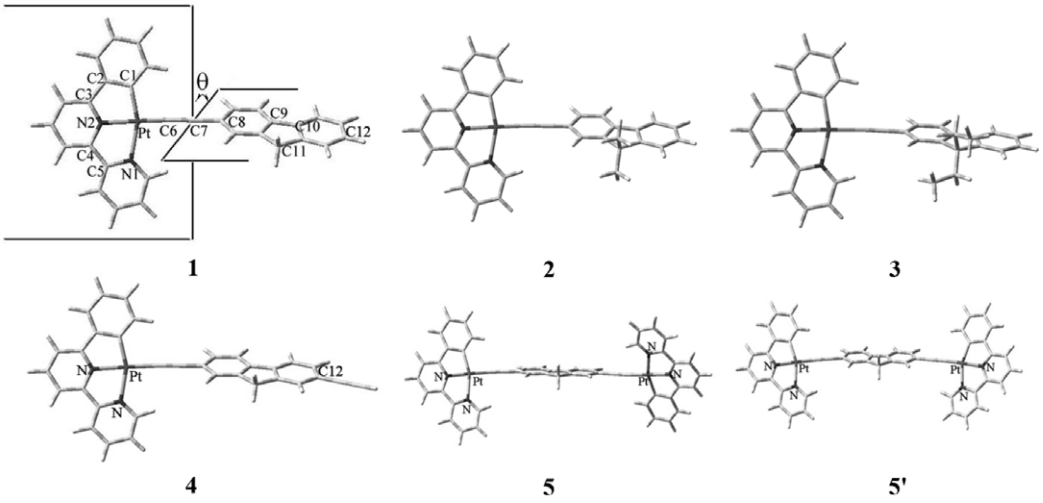

Fig. 1. Optimized molecular structures in the ground state.

Table 1
Partial optimized geometric structural parameters of the complexes in the ground and excited states associated with the experimental values of **2** and the analogues complexes.

	1 State		**2** State		*Exp*[a]	*Exp*	**3** State		**4** State		**5** State		**5′** State	
	^{1}A	^{3}A	^{1}A	^{3}A			^{1}A	^{3}A	^{1}A	^{3}A	^{1}A	^{3}B	^{1}A'	^{3}A"
Bond lengths (Å)														
Pt–N1	2.085	2.127	2.079	2.127	2.042	2.123[b]	2.080	2.126	2.085	2.128	2.085	2.083	2.085	2.087
Pt–N2	2.029	2.046	2.025	2.046	1.984	1.987[b]	2.025	2.045	2.029	2.047	2.028	2.026	2.027	2.022
Pt–C1	2.057	2.070	2.067	2.070	2.069	1.992[b]	2.068	2.071	2.057	2.070	2.056	2.071	2.056	2.068
Pt–C6	1.964	2.006	1.964	2.006	1.956	1.970[b] (2.014[c])	1.965	2.006	1.964	2.009	1.964	1.939	1.963	1.940
C2–C3	1.468	1.478	1.469	1.478	1.472		1.469	1.471	1.468	1.478	1.469	1.472	1.468	1.472
C4–C5	1.485	1.498	1.487	1.498	1.474		1.486	1.499	1.485	1.499	1.485	1.459	1.484	1.461
C6≡C7	1.228	1.220	1.228	1.220	1.210	1.185[b] (1.209[c])	1.228	1.221	1.229	1.214	1.228	1.242	1.229	1.243
C7–C8	1.425	1.397	1.425	1.397	1.433	1.424[c]	1.425	1.398	1.424	1.410	1.425	1.397	1.424	1.396
C9–C10	1.467	1.418	1.467	1.418	1.472	1.472[d]	1.467	1.419	1.464	1.406	1.464	1.434	1.463	1.432
Bond angles (°)														
N1–Pt–N2	77.1	81.5	78.1	81.5	80.9	78.4[b]	78.1	82.5	77.1	76.5	77.1	77.4	77.1	77.5
N2–Pt–C1	81.9	76.5	81.4	76.5	79.8	82.1[b]	81.5	76.5	81.9	81.5	81.9	81.5	81.9	81.7
C1–Pt–C6	100.3	98.8	99.1	99.4	102.2		99.0	98.6	99.2	99.5	98.6	99.1	98.9	99.1
Dihedral angle (°)														
θ[e]	65.2	28.9	66.5	28.9	70.0		71.3	32.7	64.5	75.1	58.8	45.2	38.9	1.1

[a] Experimental values of **2** come from Ref. [63].
[b] From Pt(C^N^N)C≡CPh in Refs. [33,66].
[c] From *trans*-[–Pt(PBu$_3$)$_2$C≡CRC≡C–]$_n$ in Ref. [48].
[d] From polyfluorene in Refs. [99,100].
[e] As shown in Fig 1.

nanthroline), which exhibits intense emission with metal-to-ligand ^{3}[Pt(5d) → π^* (phen)] charge transfer character in fluid solution [42]. Recently, they also developed tridentate cyclometalated Pt(II) lumophores with C^N^N ligand (HC^N^N = 6-aryl-2,2′-bipyridine) [33,54–58]. Compared to N^N^N (or tpy, 2,2′,6′,2″-terpyridine) and C^N^C (HC^N^CH = 2,6-diphenylpyridine) congeners [59–62], two advantages of the C^N^N ligand have emerged: the strongly σ-donating carbanion would increase the energy difference between the ligand field and the MLCT states with superior emissive properties, and associating with the anionic alkynyl ligand affords neutrality to the cyclometalated Pt(II) σ-alkynyl moiety framework. Seneclauze and Ziessel have developed various combinations of mono- or diethynyl-substituted fluorene building blocks connected via a σ-bonded ethynyl linkage to *ortho*-metallated Pt(C^N^N) segments [63]. By the general discussion, the luminescent behaviors of this kind of complexes would be assigned to triplet ligand to ligand charge transfer (LLCT) transition perturbed by some MLCT transition. In addition, such complexes are also "push–pull" type molecules as the acceptor–(π-conjugate bridge)–donor structure [64,65]. Therefore, the nonlinear optical (NLO) response for this kind of materials is interesting and an important topic, though the donor group is generally acted by transition-metal segments.

Nowadays, theoretical chemical calculations have been proved to be useful for gaining insight into the optoelectronic properties of transition–metallic complexes [66–71]. Hence, in this work, we study the mechanism of charge transfer, the more particular description of linear and nonlinear optical properties for several mono- and dinuclear tridentate cyclometalated platinum(II) σ-acetylide complexes bearing fluorene substituents (Chart 1), [Pt(C^N^N)(C≡CR)] (**1**–**3**), [Pt(C^N^N)(C≡CRC≡CH)] (**4**), [Pt(C^N^N)(C≡CRC≡C)Pt(C^N^N)] (**5**, C_2 symmetry, and **5′**, C_s symmetry), where HC^N^N = 6-aryl-2,2′-bipyridine, R = fluorene-2,7-diyl **1**, **4**, **5** and **5′**, R = 9,9-dimethylfluorene-2,7-diyl **2**, R = 9,9-diethylfluorene-2,7-diyl **3**.

2. Computational details

Density functional theory (DFT) [72,73] was applied here for the geometry optimization and electronic structure calculations of the objected complexes. The geometry structures of the complexes were optimized by employing the Becke's 3-parameter hybrid method and the Lee–Yang–Parr correlation functional (B3LYP) [74–78] with the effective core potential (ECP) basis set of the LanL2DZ [79–81] type with an additional *f*-polarization function (f = 0.18) for the Pt atom and 6-31G (d) [82] basis set for the other atoms. This kind of theoretical approach and calculation level has been proven to be reliable by previous works [83–87].

Using the respective optimized equilibrium geometry of the complexes, time-dependent density functional theory (TD-DFT) [88–92] at the B3LYP level was employed to predict their absorptions and emissions, and also the electronic properties along with static first hyperpolarizabilities [93] was calculated at the same functional level. Considering the different behaviors of the absorp-

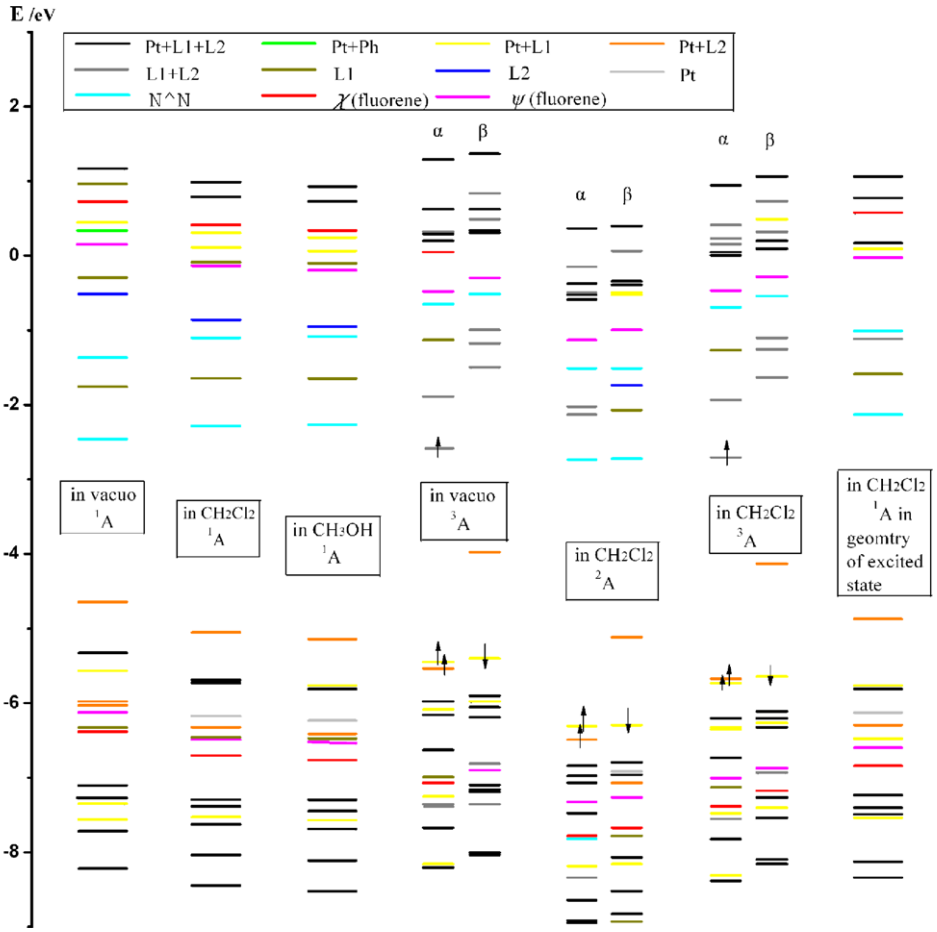

Fig. 2. Energy level diagram (in eV) of frontier orbitals calculated in different surroundings for **2** in the ground state (^{1}A) and in the oxidized state (^{2}A) as well as in the lowest triplet state (^{3}A). χ (fluorene) and ψ (fluorene): the two orbitals localized on the fluorene fragment with a and b symmetry, respectively. Correlations between orbitals of the same type are evidenced.

tion and emission of the complexes in the gas phase and solution, the solvent effects in CH_2Cl_2 and CH_3OH were taken into account by means of the polarizable continuum model (PCM) [94,95]. The 18-VE (valence electron) quasi-relativistic pseudopotential and basis set of Andrae et al. [96] with an additional *f*-polarization function ($f = 0.14$) [97] for Pt atom and the 6-31G (3df,3pd) basis set for all other atoms were used in the calculation of the ionization potentials, electron affinities, TD-DFT and static first hyperpolarizability calculations.

The static first hyperpolarizability is noted as

$$\beta_0 = (\beta_x^2 + \beta_y^2 + \beta_z^2)^{1/2} \quad (1)$$

where

$$\beta_i = 3(\beta_{iii} + \beta_{ijj} + \beta_{ikk})/5 \quad i,j,k = x,y,z.$$

All of the calculations in this work were carried out using the GAUSSIAN 03 program package [98].

3. Results and discussion

3.1. Geometric structures in the Ground state and the lowest triplet states

The geometry optimization of mono- and di-nuclear Pt(II) complexes with the electron-rich fluorene was performed by the B3LYP functional in the ground state. The optimized geometry structures of the complexes in ground state are depicted in Fig. 1. Complex **5** and **5′** are a pair of dinuclear geometrical isomers, which were restricted to C_2 and C_s symmetries, respectively.

From optimized molecular geometries, the Pt(C^N^N)-acetylide fragment is square-planar conformation whereas the fluorene group is titled out of the plane. Except the difference of the dihedral angle (θ, as shown in Fig. 1), the structural parameters in **1**–**3** are almost same. The partial optimized structural parameters and related experimental values (X-ray crystallographic data (CIF)) of **2**, Pt(C^N^N)C≡CPh (HC^N^N = 6-aryl-2,2'-bipyridine) [33,66], *trans*-[–Pt(PBu$_3$)$_2$C≡CRC≡C–]$_n$ (R = 9,9-dimethylfluorene-2,7-diyl) [48], and polyfluorene [99,100], are listed in Table 1. The calculated Pt–N distances of 2.02–2.08 Å are all slightly longer than the observed values of 1.98–2.04 Å in experiments. Compared with the previous calculated bond lengths of Pt(C^N^N)C≡CPh [33,66], the N1 atom side of C^N^N ligand are more closer to Pt atom center in **1–5**. The calculated Pt–C6 is shorter and the C6≡C7 is longer for **1**–**5** than those for Pt(C^N^N)C≡CPh and *trans*-[–Pt(PBu$_3$)$_2$C≡CRC≡C–]$_n$ (R = 9,9-dimethylfluorene-2,7-diyl). It is noted that the C9–C10 contacts (1.467 Å) are stronger in **1**–**5** than in polyflourene (1.472 Å). The character of bond lengths illustrates that, in **1**–**5**, the metal–ligand interactions are strengthened whereas the C≡C bonds are weakened. The coordination geometry of Pt(II) exhibits a quasi-square-planar conformation, where there is ca. 9–14° deviation of the N1–Pt–N2 and N2–Pt–C1 bond angles from 90°, which agree well with the experimental case. The fluorene fragment of **2** is tilted out of the quasi-square-plane by 70.0° in experimental

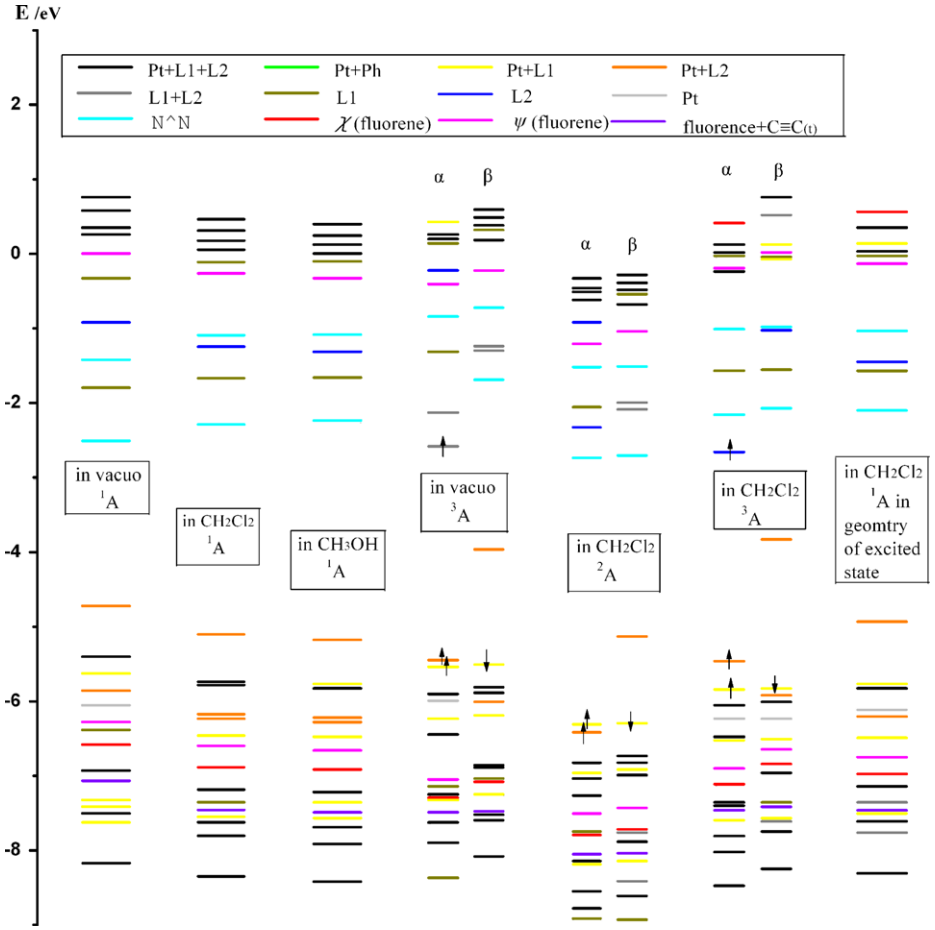

Fig. 3. Energy level diagram (in eV) of frontier orbitals calculated in different surroundings for **4** in the ground state (^{1}A) and in the oxidized state (^{2}A) as well as in the lowest triplet state (^{3}A). χ (fluorene) and ψ (fluorene): the two orbitals localized on the fuorene fragment with a and b symmetry, respectively. C≡C$_{(t)}$: the terminal alkynyl. Correlations between orbitals of the same type are evidenced.

measurement. In the calculations, the dihedral angles (θ) of **1**–**3** are 65.2°, 66.5°, and 71.3°, respectively, while in **5** and **5′**, the θ is reduced to 59° and 39°, respectively.

Upon excitation, several notable conclusions can be drawn from the results in Table 1. (1) The interaction between metal and C^N^N ligand of **1**–**4** is weakened in the lowest triplet state (Pt–N distances elongated by 0.2–0.5 Å and Pt–C1 distances elongated slightly comparing with that in ground state), whereas no remarkable variation is found in **5** and **5′**. (2) Elongated Pt–C6 bond lengths and shortened C6≡C7 triplet bond distance in **1**–**4** are observed, while the reverse results occur in **5** and **5′**. (3) The dihedral angles (θ), except **4**, have reduced trends, and the whole molecule of **5′** is even almost coplanar. Therefore, upon the excitation, the characters of the CT transitions for mono- and dinuclear complexes should be somewhat different.

3.2. Orbital analysis and electronic properties

Firstly, we depict the Kohn–Sham molecular orbitals (MO) and discuss the electronic properties for the complexes. The energy diagrams of frontier orbitals of **2**, **4**, **5**, and **5′** in ground state, ionized ground doublet state and excited state are given in Figs. 2–5, and a correlation of the system in different solvents or between the ground state and the lowest-energy triplet excited state is established. As will be seen later, these MOs provide the information of the excited state described by TD-DFT. To discuss conveniently, some typical MOs are presented in Fig. 6, where the C^N^N ligand and [–C≡C–fluorene] ligand ([–C≡C–fluorene–C≡C–] for **4**, **5** and **5′**) are noted by L_1 and L_2, respectively. Because bearing much similarity in MOs with **2**, those of **1** and **3** are not listed.

See Fig. 2, most of the higher occupied MOs of **2** exhibit the metal d_π and L_2 ligand character. The HOMO orbital of **2** is composed of 16% Pt (d_{xy}) and 77% L_2 (C≡C: 27%) ligand, while the LUMO, lying above the HOMO by about 2.20 eV, is mainly localized upon the bipyridine segment of C^N^N ligand (91%). The LUMO+2 of **2** has almost the same components and antibonding (π^*) characters as the LUMO, while LUMO+1 is delocalized on the C^N^N ligand. We choose dichloromethane and methanol medium to investigate the environmental effects. The Mulliken charges on each fragment for the complexes are given in Table 2. The platinum and alkynyl fragments retain prominent positive and negative charge, respectively, and turn to be more negative with the increase of the solvent polarity. In contrast, the charge of pyridyl moieties positively rises. This fact means that as the increase of the solvent polarity, the interaction between the system and solvent molecule is enhanced [101]. Charge separation is also reflected by the increase in dipole moment from 9.7 D in vacuo to 13.1 D (in dichloromethane) and 13.7 D (in methanol) in polar solvents (see Table 3). The electrostatic solvation energy takes on a trend that the solvated molecules are even more stabilized. According to above discussion, the MOs mainly composed by metal and L_2 are stabilized, while the energy levels of LUMO to LUMO+2 with L_1 or N^N (bipyridine) π^* components increase in the polarized solvents. Under the same media with **1**, the dipole moment, salvation energy, and

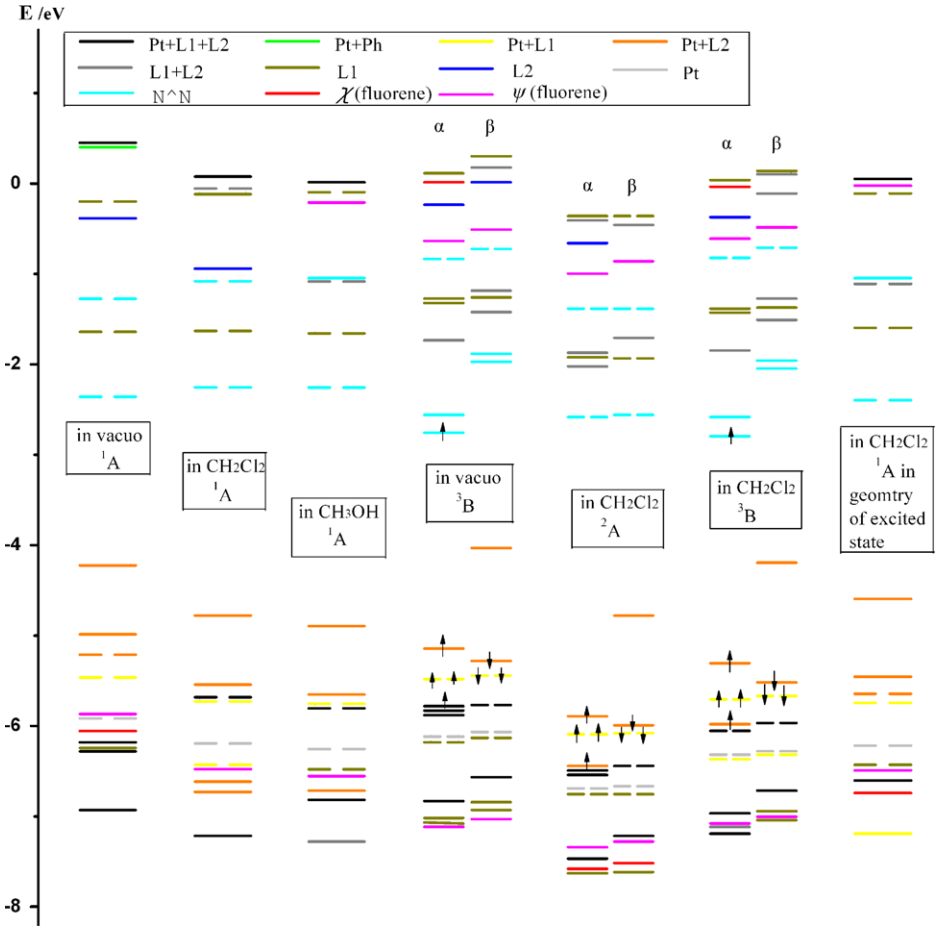

Fig. 4. Energy level diagram (in eV) of frontier orbitals calculated in different surroundings for **5** in the ground state (^{1}A) and in the oxidized state (^{2}A) as well as in the lowest triplet state (^{3}B). χ (fluorene) and ψ (fluorene): the two orbitals localized on the fluorene fragment with a and b symmetry, respectively. Correlations between orbitals of the same type are evidenced.

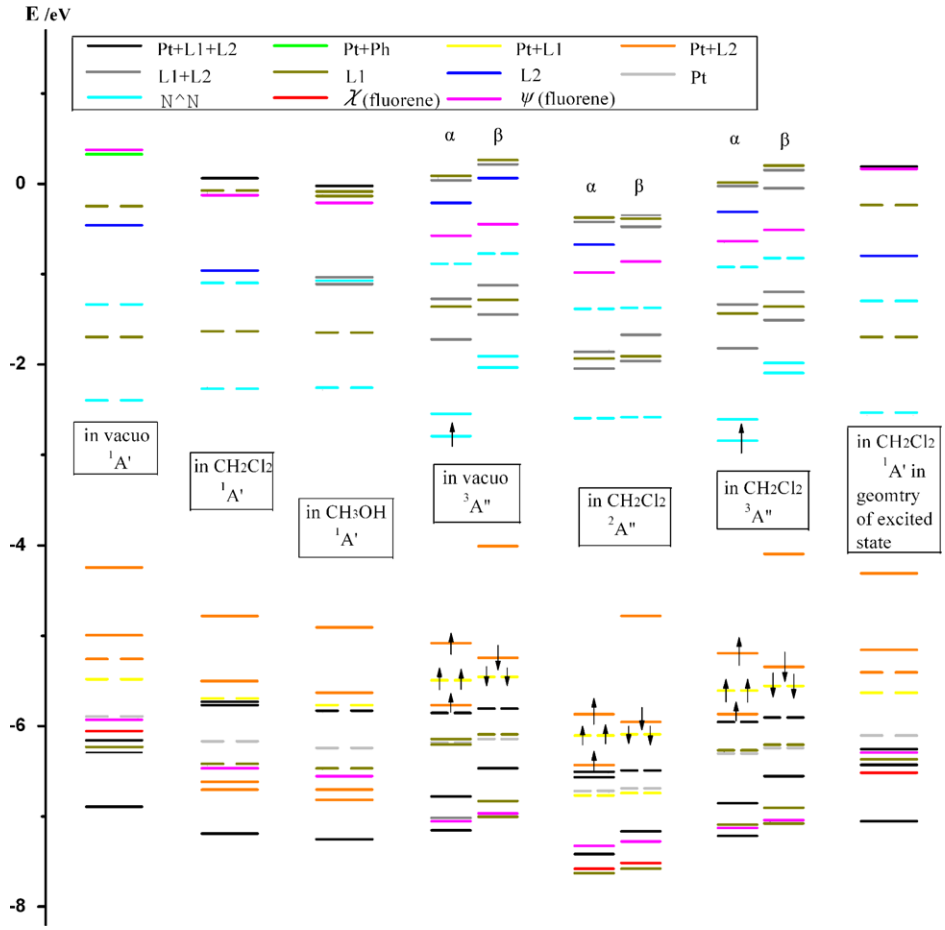

Fig. 5. Energy level diagram (in eV) of frontier orbitals calculated in different surroundings for **5′** in the ground state (^{1}A') and in the oxidized state (^{2}A") as well as in the lowest triplet state (^{3}A"). χ (fluorene) and ψ (fluorene): the two orbitals localized on the fluorene fragment with a and b symmetry, respectively. Correlations between orbitals of the same type are evidenced.

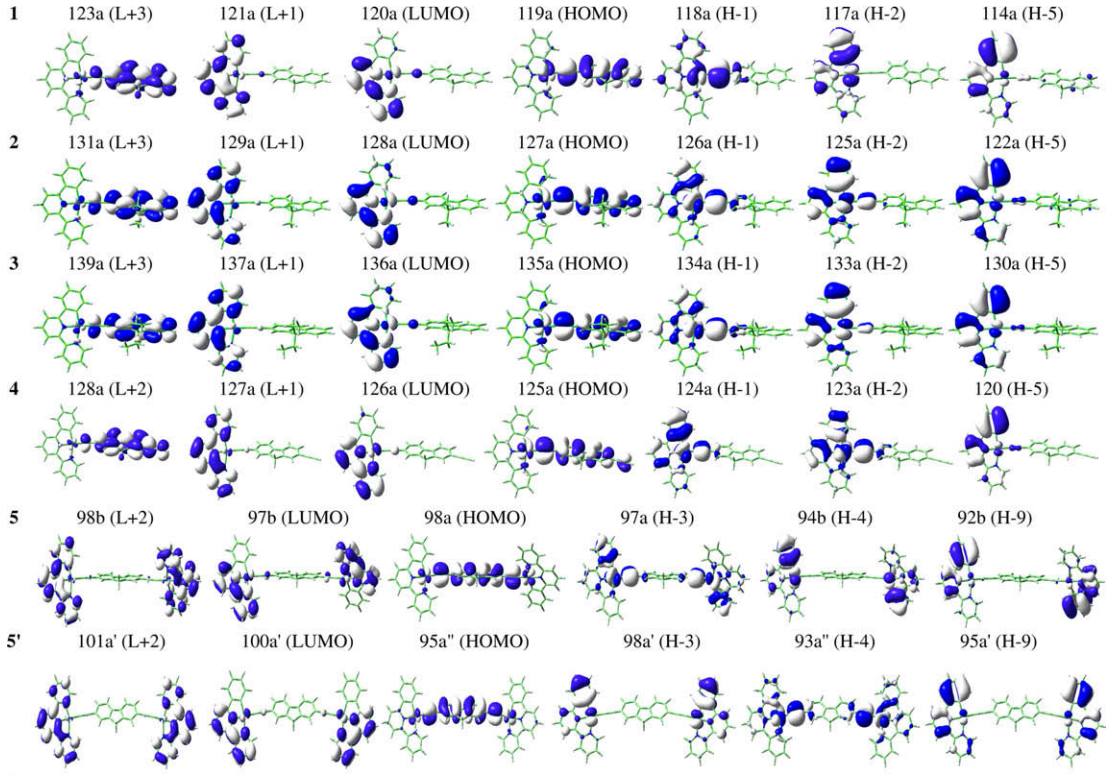

Fig. 6. Several important molecular orbitals calculated in CH_2Cl_2 in the ground state.

Table 2
Mulliken charges for different fragments of the complexes calculated in different surroundings (vacuum and two solvent (CH_2Cl_2: $\varepsilon = 8.93$; CH_3OH: $\varepsilon = 32.63$)).

	Fragment	Ground state			Oxidized form		Reductive form		Excited state	
		Vacuum	CH_2Cl_2	CH_3OH	Vacuum	CH_2Cl_2	Vacuum	CH_2Cl_2	Vacuum	CH_2Cl_2
1	Pt	0.736	0.636	0.615	0.862	0.814	0.648	0.483	0.723	0.603
	Pyridyl (c)[a]	−0.065	0.010	0.024	0.024	0.059	−0.345	−0.304	−0.160	−0.134
	Pyridyl (p)[b]	0.119	0.175	0.184	0.185	0.217	−0.247	−0.194	−0.028	0.013
	Phenyl	−0.267	−0.292	−0.294	−0.207	−0.254	−0.422	−0.405	−0.313	−0.334
	C≡C	−0.514	−0.525	−0.530	−0.369	−0.369	−0.505	−0.528	−0.385	−0.404
	Fluorene	−0.009	−0.004	0.001	0.505	0.533	−0.129	−0.052	0.162	0.255
2	Pt	0.735	0.634	0.613	0.860	0.812	0.646	0.481	0.721	0.601
	Pyridyl (c)[a]	−0.065	0.010	0.024	0.024	0.059	−0.345	−0.304	−0.160	−0.134
	Pyridyl (p)[b]	0.119	0.175	0.184	0.185	0.217	−0.247	−0.194	−0.028	0.013
	Phenyl	−0.267	−0.292	−0.294	−0.207	−0.254	−0.422	−0.405	−0.313	−0.333
	C≡C	−0.514	−0.525	−0.528	−0.367	−0.367	−0.505	−0.528	−0.383	−0.403
	Fluorene	−0.008	−0.002	0.001	0.505	0.533	−0.127	−0.050	0.162	0.255
3	Pt	0.734	0.635	0.615	0.861	0.814	0.645	0.481	0.721	0.601
	Pyridyl (c)[a]	−0.064	0.010	0.024	0.025	0.058	−0.345	−0.304	−0.160	−0.134
	Pyridyl (p)[b]	0.121	0.175	0.182	0.186	0.217	−0.247	−0.194	−0.028	0.013
	Phenyl	−0.266	−0.291	−0.292	−0.208	−0.254	−0.422	−0.405	−0.313	−0.330
	C≡C	−0.514	−0.522	−0.527	−0.368	−0.367	−0.502	−0.527	−0.385	−0.404
	Fluorene	−0.011	−0.006	0.001	0.504	0.532	−0.127	−0.051	0.161	0.257
4	Pt	0.737	0.639	0.617	0.854	0.808	0.652	0.486	0.713	0.616
	Pyridyl (c)[a]	−0.062	0.011	0.025	0.021	0.059	−0.339	−0.302	−0.126	0.010
	Pyridyl (p)[b]	0.121	0.176	0.185	0.182	0.216	−0.239	−0.191	0.010	0.166
	Phenyl	−0.266	−0.291	−0.293	−0.210	−0.254	−0.418	−0.404	−0.293	−0.280
	C≡C	−0.512	−0.522	−0.527	−0.376	−0.373	−0.501	−0.524	−0.408	−0.456
	Fluorene	0.053	0.062	0.067	0.493	0.544	−0.047	0.018	0.158	0.031
	C≡C(t)[c]	−0.071	−0.075	−0.074	0.036	0.001	−0.107	−0.082	−0.054	−0.087
5	Pt	1.470	1.272	1.230	1.609	1.466	1.377	1.325	1.543	1.342
	Pyridyl (c)[a]	−0.139	0.017	0.047	−0.011	0.079	−0.433	−0.390	−0.300	−0.217
	Pyridyl (p)[b]	0.235	0.349	0.367	0.318	0.396	−0.145	−0.122	−0.052	0.044
	Phenyl	−0.540	−0.586	−0.589	−0.466	−0.544	−0.699	−0.700	−0.610	−0.639
	C≡C	−1.033	−1.052	−1.061	−0.854	−0.870	−1.036	−1.033	−0.867	−0.892
	Fluorene	0.007	−0.001	0.006	0.405	0.473	−0.064	−0.080	0.285	0.363
5′	Pt	1.473	1.274	1.231	1.611	1.474	1.379	1.326	1.547	1.513
	Pyridyl (c)[a]	−0.142	0.015	0.045	−0.009	0.081	−0.433	−0.390	−0.296	−0.280
	Pyridyl (p)[b]	0.226	0.345	0.364	0.311	0.391	−0.149	−0.122	−0.039	−0.011
	Phenyl	−0.541	−0.587	−0.591	−0.463	−0.543	−0.700	−0.702	−0.613	−0.623
	C≡C	−1.036	−1.056	−1.063	−0.855	−0.872	−1.039	−1.036	−0.872	−0.873
	Fluorene	0.020	0.009	0.014	0.405	0.468	−0.058	−0.076	0.273	0.274

[a] The central pyridyl.
[b] The peripheral pyridyl.
[c] The terminal alkynyl.

HOMO–LUMO energy gap of **4** increases 1 D, about 1 kcal/mol, and 0.02 eV, respectively, in comparison with **1**. The terminal ethynyl at fluorene is different from that one linked to the Pt atom, and can hardly lead to any significant change in property. Fig. 3 shows that the HOMO−9 of **4** is mainly composed of the fluorene and terminal ethynyl fragment. It can be seen that the HOMO and HOMO−1 of dinuclear complexes **5** and **5′** are contributed by the metal and L_2 fragment. The solvation energies of **5** and **5′** are remarkable augmented in comparison with **1**–**4**, since the interaction surface between the complex and the solvent molecule is extended. Moreover, the energy gaps of **5** and **5′** decrease 0.2–0.3 eV relative to the mono-nuclear complexes.

Because photophysical experiments may involve the ground doublet state as a result of the oxidization and reduction, the ionization potentials (IP), electron affinities (EA) are taken into

Table 3
Dipole moment μ, electrostatic solvation energy $E_{(S)}$ and the HOMO–LUMO energy gap ΔE calculated in different surroundings for each molecule.

	Medium	μ (D)	$E_{(S)}$ (kcal/mol)	ΔE (eV)
1	Vacuum	9.7	0	2.20
	CH_2Cl_2	13.1	−18.0	2.78
	CH_3OH	13.7	−21.9	2.88
2	Vacuum	9.7	0	2.20
	CH_2Cl_2	13.1	−17.7	2.77
	CH_3OH	13.8	−21.8	2.88
3	Vacuum	9.8	0	2.19
	CH_2Cl_2	13.1	−17.4	2.76
	CH_3OH	13.8	−21.7	2.87
4	Vacuum	10.8	0	2.22
	CH_2Cl_2	14.3	−19.2	2.80
	CH_3OH	14.9	−23.3	2.90
5	Vacuum	8.6	0	1.85
	CH_2Cl_2	12.2	−32.2	2.52
	CH_3OH	12.8	−39.2	2.64
5′	Vacuum	12.8	0	1.83
	CH_2Cl_2	18.2	−32.3	2.51
	CH_3OH	19.1	−39.3	2.63

Table 4
Ionization potentials (IP), electron affinities (EA), and the HOMO, LUMO energy levels for each molecule calculated in the gas phase and CH_2Cl_2 solution.

	$IP_{(g)}$	$EA_{(g)}$	$IP_{(s)}$	$EA_{(s)}$	$E_{HOMO(g)}$	$E_{LUMO(g)}$	$E_{HOMO(s)}$	$E_{LUMO(s)}$
1	5.91	−1.11	5.08	−2.27	−4.65	−2.45	−5.05	−2.27
2	5.89	−1.12	5.06	−2.27	−4.65	−2.46	−5.04	−2.27
3	5.87	−1.12	5.07	−2.28	−4.64	−2.45	−5.03	−2.27
4	5.92	−1.17	5.10	−2.28	−4.72	−2.50	−5.08	−2.28
5	5.23	−1.49	4.79	−0.98	−4.21	−2.36	−4.78	−2.26
5′	5.24	−1.51	4.79	−1.01	−4.24	−2.41	−4.79	−2.28

In eV.

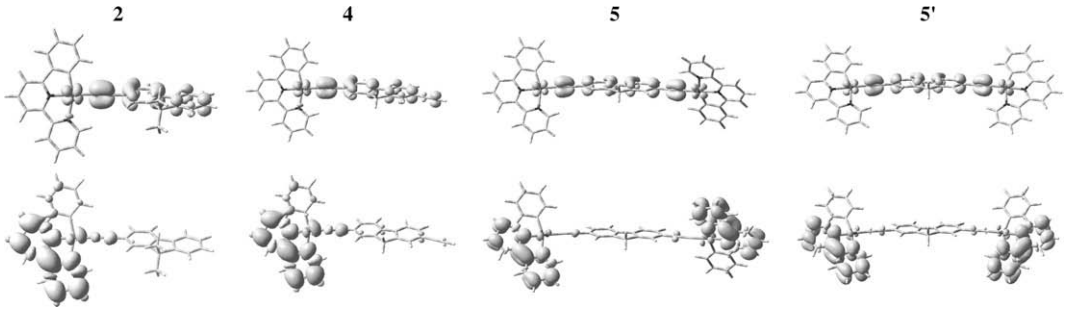

Fig. 7. Spin density distribution for the oxidized forms (top) and the reduced forms (bottom) of **2**, **4**, **5**, and **5′** calculated in CH_2Cl_2.

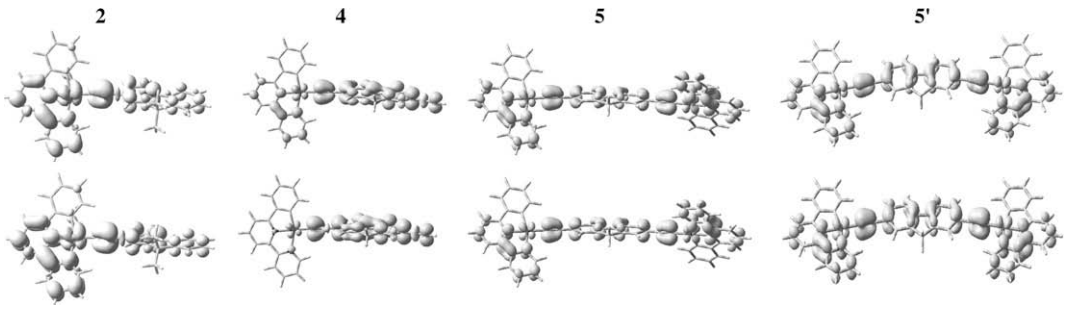

Fig. 8. Spin density distribution for the lowest triplet states of **2**, **4**, **5**, and **5′** calculated in vacuo (top) and CH_2Cl_2 (bottom).

account and the values are listed in Table 4, which were obtained by the differences of the total self-consistent energies of the ground doublet states of the oxidized form or the reductive form and of the ground state. Figs. 2–5 reveal that the depopulated β LUMOs are spin orbitals composed by Pt and L_2 fragment. This expresses that the oxidation has occurred on the metal ion and L_2 ligand. The Mulliken analysis proofed this proposed oxidation course, which shows over 85% positive charge of the cation is populated on the metal and L_2 ligand. The positive charge on the Pt and the fluorene increases when the ionization occurs in CH_2Cl_2 solution. Due to the higher energy levels of HOMO in the dinuclear complexe of **5** and **5′**, the corresponding IP decreased by 0.65 eV in contrast to the mono-nuclear complexes. Compared with the IP value of the polyfluorene material (5.37 eV) [99,100], the present complexes are more stable in the gas phase. The EA values of the mononuclear complexes are about 1.1 eV in vacuo and 2.3 eV in CH_2Cl_2, while the EA values of **5** and **5′** are about 1.0 eV in solution, the change is because that the reducing charge is localized on the N^N moiety in dinuclear complexes and is different from **1**–**4** which occur on the metal atom and tridentate C^N^N ligand. The spin density contours are shown in Fig. 7.

An elegant way to describe the electronic redistribution upon triplet formation is to examine the MO location of in the ground-, excited-, and oxidized state. Compared the ground state and triplet state of **2**, the lowest α-vacant π^* is stabilized and acts as an electron acceptor, which is delocalized on the L_1 and L_2 ligands, while the highest occupied β spin orbital ($d_\pi + L_2$) rises in energy and is depopulated in triplet state. Thus, the lowest triplet state is generated mainly by the promotion of an electron from [d_π (Pt) + L_2] to L_1 fragment. The identical triplet-state character was calculated in vacuo, and its total energy is larger than that in solution by 13.4 kcal/mol. The resulting spin density distribution of the ^{3}A excited state is shown in Fig. 8. The energy diagram also points out that the occupied orbitals are stabilized in the ^{3}A excited state and the energies of the orbitals with fluorene character descend as a consequence of the electron transfer. The composition of metal and L_1 in the higher occupied orbitals greatly increase. The stabilized effects are more evident in the oxidized state than in the triplet state, because of the more intense depopulation in the oxidized ^{2}A state [102,103]. For **4** in polar solvent, α-type HOMO is mainly localized on the extended L_2 ligand and ^{3}A state can be characterized as $^3[\pi \rightarrow \pi^*]/^3ML_2CT$ state. This is different from the nature of the ^{3}A state in vacuo ($^3L_2L_1CT/^3ML_1CT/^3IL_2CT$) because of the polar solvent increases the electronic localization. For dinuclear complexes **5** and **5′**, triplet state exhibits a mixing of $^3L_2L_1CT$ and $^3ML_1CT$ character, and the α-type HOMOs are a π^* orbital developed on the N^N moieties. From the Mulliken charge analysis, the charge transfer from ground state to triplet state in **5** and **5′** (e.g. −0.001 to 0.363 at fluorene of **5** in CH_2Cl_2, 0.366 to −0.173 at bipyridyl of **5** in CH_2Cl_2) are much more than that in **1**–**4** (e.g. −0.004 to 0.162 at fluorene of **1** in CH_2Cl_2, 0.185 to −0.121 at bipyridyl of **1** in CH_2Cl_2). This is duo to the more intense electronic delocalization effect imported by the second Pt moiety. For the isomers, there is 0.07 and 0.24 charge transfer magnitude at Pt in **5** and **5′**, respectively, since the molecular geometry of **5′** is more planar than **5**.

3.3. Absorption and emission

The low-lying singlet excited states of these complexes based on their ground-state geometry with vacuum or solvent surroundings were studied using time-dependent DFT (TD-DFT) method in which the vertical excitation energies from the ground state were calculated. For the absorptions of **1**–**5** in CH_2Cl_2, the corresponding transitions with dominant electric dipole oscillator strength values are reported in Table 5. Based on the excitation energies and oscillator strength values, the absorptions of **1**–**5** are simulated by Gaussian-type curves [71], the curves associated with the corresponding experimentally measured absorption spectra in CH_2Cl_2 solution at room temperature are shown in Fig. 9. The solvent effects on the adsorptions in each complex are presented in Fig. 10. To gain reasonable Stokes shifts, the TD-DFT and ΔSCF (self-consis-

Table 5
Absorptions of the complexes in CH_2Cl_2 solution according to the TD-DFT calculations. f: oscillator strength.

	Transition		$\psi_o \rightarrow \psi_v$ (CI coefficient)[a]	E_{ver} (nm (eV))	f	Assignment[b]
1	$X^1A \rightarrow A^1A$	H → L	119a → 120a (0.69)	550.2 (2.25)	0.0567	L_2L_1CT/ML_1CT
	$X^1A \rightarrow B^1A$	H-1 → L	118a → 120a (0.57)	441.3 (2.81)	0.1087	ML_1CT/L_2L_1CT
		H-2 → L	117a → 120a (0.35)			ML_1CT/IL_1CT
	$X^1A \rightarrow C^1A$	H-1 → L	118a → 121a (0.55)	358.2 (3.46)	0.2712	ML_1CT/L_2L_1CT
		H-2 → L+1	117a → 121a (0.31)			$ML_1CT/\pi(L_1) \rightarrow \pi^*(L_1)$
	$X^1A \rightarrow D^1A$	H-5 → L	114a → 120a (0.65)	339.6 (3.65)	0.1494	$IL_1CT/\pi(L_1) \rightarrow \pi^*(L_1)$
	$X^1A \rightarrow E^1A$	H → L+3	119a → 123a (0.63)	327.7 (3.78)	1.0306	$\pi(F) \rightarrow \pi^*(F)/IL_2CT$
	$X^1A \rightarrow F^1A$	H-5 → L+1	114a → 121a (0.60)	286.6 (4.33)	0.1282	$\pi(L_1) \rightarrow \pi^*(L_1)/IL_1CT$
2	$X^1A \rightarrow A^1A$	H → L	127a → 128a (0.69)	551.7 (2.25)	0.0595	L_2L_1CT/ML_1CT
	$X^1A \rightarrow B^1A$	H-1 → L	126a → 128a (0.58)	441.8 (2.81)	0.1080	ML_1CT/L_2L_1CT
		H-2 → L	125a → 128a (0.33)			ML_1CT/IL_1CT
	$X^1A \rightarrow C^1A$	H-1 → L	126a → 129a (0.53)	358.6 (3.46)	0.2737	ML_1CT/L_2L_1CT
		H-2 → L+1	125a → 129a (0.33)			$ML_1CT/\pi(L_1) \rightarrow \pi^*(L_1)$
	$X^1A \rightarrow D^1A$	H-5 → L	122a → 128a (0.65)	340.0 (3.65)	0.1570	$IL_1CT/\pi(L_1) \rightarrow \pi^*(L_1)$
	$X^1A \rightarrow E^1A$	H → L+3	127a → 131a (0.63)	330.4 (3.76)	0.9609	$\pi(F) \rightarrow \pi^*(F)/IL_2CT$
	$X^1A \rightarrow F^1A$	H-5 → L+1	122a → 129a (0.60)	286.9 (4.32)	0.1234	$\pi(L_1) \rightarrow \pi^*(L_1)/IL_1CT$
3	$X^1A \rightarrow A^1A$	H → L	135a → 136a (0.69)	556.9 (2.23)	0.0398	L_2L_1CT/ML_1CT
	$X^1A \rightarrow B^1A$	H-1 → L	134a → 136a (0.63)	440.6 (2.81)	0.1372	ML_1CT/L_2L_1CT
		H-2 → L	133a → 136a (0.23)			ML_1CT/IL_1CT
	$X^1A \rightarrow C^1A$	H-1 → L+1	134a → 137a (0.46)	358.3 (3.46)	0.3141	ML_1CT/L_2L_1CT
		H-2 → L+1	133a → 137a (0.45)			$ML_1CT/\pi(L_1) \rightarrow \pi^*(L_1)$
	$X^1A \rightarrow D^1A$	H-5 → L	130a → 136a (0.66)	340.3 (3.64)	0.1677	$IL_1CT/\pi(L_1) \rightarrow \pi^*(L_1)$
	$X^1A \rightarrow E^1A$	H → L+3	135a → 139a (0.64)	331.2 (3.74)	1.0147	$\pi(F) \rightarrow \pi^*(F)/IL_2CT$
	$X^1A \rightarrow F^1A$	H-5 → L+1	130a → 137a (0.60)	286.8 (4.32)	0.1566	$\pi(L_1) \rightarrow \pi^*(L_1)/IL_1CT$
4	$X^1A \rightarrow A^1A$	H → L	125a → 126a (0.69)	542.4 (2.29)	0.0701	L_2L_1CT/ML_1CT
	$X^1A \rightarrow B^1A$	H-2 → L	123a → 126a (0.59)	439.1 (2.82)	0.1468	ML_1CT/L_2L_1CT
		H-1 → L	124a → 126a (0.32)			ML_1CT/IL_1CT
	$X^1A \rightarrow C^1A$	H → L+2	125a → 128a (0.48)	362.4 (3.42)	0.9641	$\pi(F) \rightarrow \pi^*(F)/IL_2CT$
		H-1 → L+1	124a → 127a (0.34)			$\pi(L_1) \rightarrow \pi^*(L_1)/ML_1CT$
		H-2 → L+1	123a → 127a (0.31)			$ML_1CT/L_2L_1CT/\pi(L_1) \rightarrow \pi^*(L_1)$
	$X^1A \rightarrow D^1A$	H-1 → L+1	124a → 127a (0.39)	349.1 (3.55)	0.1606	$\pi(L_1) \rightarrow \pi^*(L_1)/ML_1CT$
		H → L+2	125a → 128a (0.33)			$\pi(F) \rightarrow \pi^*(F)/IL_2CT$
	$X^1A \rightarrow E^1A$	H-5 → L	120a → 126a (0.66)	340.4 (3.64)	0.1767	$IL_1CT/\pi(L_1) \rightarrow \pi^*(L_1)$
	$X^1A \rightarrow F^1A$	H-5 → L+1	120a → 127a (0.59)	286.6 (4.33)	0.1710	$\pi(L_1) \rightarrow \pi^*(L_1)/IL_1CT$
5	$X^1A \rightarrow A^1B$	H → L	98a → 97b (0.68)	590.6 (2.10)	0.1679	L_2L_1CT/ML_1CT
	$X^1A \rightarrow B^1B$	H-2 → L+1	95b → 99a (0.43)	444.6 (2.79)	0.3949	L_2L_1CT/ML_1CT
		H-3 → L	97a → 97b (0.37)			ML_1CT/L_2L_1CT
		H-5 → L	96a → 97b (0.26)			ML_1CT/IL_1CT
	$X^1A \rightarrow C^1B$	H-1 → L+1	96b → 99a (0.66)	428.7 (2.89)	0.0257	L_2L_1CT/ML_1CT
	$X^1A \rightarrow D^1B$	H → L+6	98a → 100b (0.49)	366.3 (3.38)	0.8242	$\pi(L_2) \rightarrow \pi^*(L_2)/IL_2CT$
		H-3 → L+2	97a → 98b (0.32)			$ML_1CT/L_2L_1CT/\pi(L_1) \rightarrow \pi^*(L_1)$
		H-2 → L+3	95b → 100a (0.30)			L_2L_1CT/ML_1CT
	$X^1A \rightarrow E^1+B$	H-5 → L+2	96a → 98b (0.45)	364.3 (3.40)	0.1605	$\pi(L_1) \rightarrow \pi^*(L_1)/ML_1CT$
		H-4 → L+3	94b → 100a (0.40)			$\pi(L_1) \rightarrow \pi^*(L_1)/ML_1CT$
	$X^1A \rightarrow F^1B$	H-8 → L	94a → 97b (0.48)	340.9 (3.64)	0.2504	$\pi(L_1) \rightarrow \pi^*(L_1)/IL_1CT$
		H-9 → L+1	92b → 99a (0.43)			$\pi(L_1) \rightarrow \pi^*(L_1)/IL_1CT$
5′	$X^1A' \rightarrow A^1A''$	H → L	95a″ → 100a′ (0.68)	587.6 (2.11)	0.3939	L_2L_1CT/ML_1CT
	$X^1A' \rightarrow B^1A''$	H → L+2	95a″ → 101a′ (0.53)	447.7 (2.77)	0.3945	L_2L_1CT/ML_1CT
		H-4 → L	93a″ → 100a′ (0.31)			L_2L_1CT/ML_1CT
		H-5 → L+1	97a′ → 96a″ (0.29)			L_2L_1CT/ML_1CT
	$X^1A' \rightarrow C^1A''$	H-1 → L+1	99a′ → 96a″ (0.67)	427.7 (2.90)	0.0349	L_2L_1CT/ML_1CT
	$X^1A' \rightarrow D^1A''$	H → L+6	95a″ → 103a′ (0.44)	365.1 (3.40)	0.6655	$\pi(L_2) \rightarrow \pi^*(L_2)$
		H-3 → L+3	98a′ → 97a″ (0.35)			$ML_1CT/\pi(L_1) \rightarrow \pi^*(L_1)$
		H-2 → L+2	94a″ → 101a′ (0.34)			$ML_1CT/\pi(L_1) \rightarrow \pi^*(L_1)$
	$X^1A' \rightarrow E^1A''$	H-4 → L+2	93a" → 101a′ (0.474)	362.7 (3.42)	0.1176	L_2L_1CT/ML_1CT
		H-5 → L+3	97a′ → 97a″ (0.41)			L_2L_1CT/ML_1CT
	$X^1A' \rightarrow F^1A'$	H-9 → L	95a′ → 100a′ (0.48)	342.2 (3.62)	0.2810	$IL_1CT/\pi(L_1) \rightarrow \pi^*(L_1)$
		H-8 → L+1	91a″ → 96a″ (0.46)			$IL_1CT/\pi(L_1) \rightarrow \pi^*(L_1)$

[a] H denotes the HOMO and L denotes the LUMO.
[b] L_1 denotes 6-aryl-2,2′-bipyridine (C^N^N) ligand and L_2 denotes [–C≡C–fluorene] or [–C≡C–fluorene–C≡C–] fragments, ILCT means the charge transfer between N^N and phenyl at L_1 ligand or between fluorene and alkynyl at L_2 ligand. The $\pi \rightarrow \pi^*$ charge transfer transition is localized on the fixed fragments in L_1 or L_2.

tent field) [104–106] methods were employed to calculate the wavelengths of phosphorescence, respectively, and the results are summarized in Table 6.

From Fig. 9, one can see that the experimental spectra are well reproduced by the present calculations but with some red shifts in wavelength for the lowest energy absorption bands (ca. 0.2 eV). The differences between calculations and experimental data for **1**–**5**, especially the lowest excited states, not only come from TDDFT limitations, but also include the minor deviation between the optimized molecular geometry and the experimentally observed results, because the TDDFT calculations are based on the optimized ground state geometries. The red shifts are tolerable for this method, especially for a spatially extended π-system [107–110]. Associated with Table 5, we sum up the main conclusions: For **1**, the lowest excited state (E_{ver} <2.5 eV) is essentially obtained from a HOMO-to-LUMO mono-excitation,

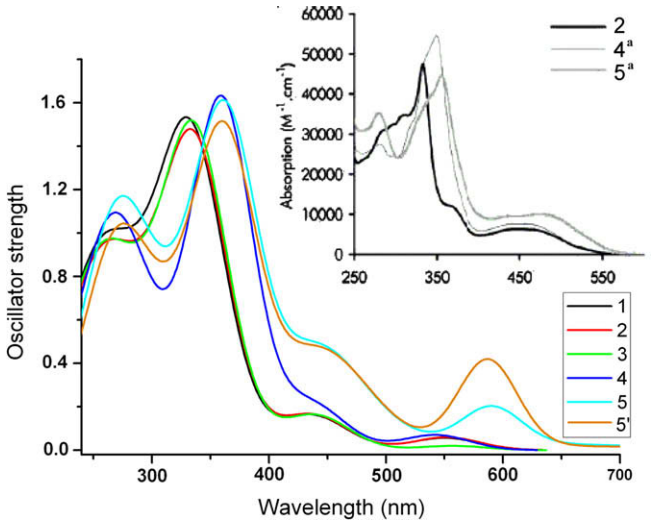

Fig. 9. Simulated absorption spectra of the complexes in CH_2Cl_2 solution compared to the experimental spectra (inset). [a]The experimental data is from the dimethyl derivatives of **4** and **5**, respectively.

the corresponding transition is a combination of L_2 ligand and metal Pt to L_1 ligand charge transfer, abbreviated as L_2L_1CT/ML_1CT. The states are dominated by electron transition from the metal to the L_1 ligand (ML_1CT) in the 350–460 nm region. The intense high energy absorption bands greater than 3.5 eV, are attributed to interligand charge transfer between phenyl and bipyridyl units in L_1 or between alkynyl and fluorenyl unit in L_2 and $\pi \rightarrow \pi^*$ charge transfer localized on the fixed fragments in L_1 and L_2. There is ca. 2–5 nm difference in the lowest energy absorptions in **1**–**3** and following the order of **3** > **2** > **1**. In **4**, when the L_2 ligand is extended by the disubstituted fluorene, a 0.04 eV blue shift of L_2L_1CT transition was noted. The IL_2CT and $\pi \rightarrow \pi^*$ (on fluorene segment) transition energies decrease 0.35 eV in contrast to **1**. The transition energies are affected by the electronic localization on the extended L_2 ligand. For the dinuclear **5** and **5′**, the lowest energy L_2L_1CT absorption bands are red shifted to around 590 nm, and the L_2L_1CT type transition appears over the 400–600 nm region. The ML_1CT transitions are expanded to higher energy level. From Fig. 9 and Table 5, it is noted that the oscillator strengths of **5** and **5′** in lower energy absorption bands are sharply enhanced, and specially, the oscillator strengths of the lowest energy absorption in **5′** is ca. 6–8 times more than the mono-nuclear analogues. The obvious intensity of the lowest energy absorption of **5′** is not reflected in experiment due to the small proportion in the dinuclear compound. In the high energy region, the absorptions of **5** are similar to **4**, but the oscillator strength of **5′** in this band is decreased slightly as there are more L_2L_1CT characters. The bathochromic shifts of **5** and **5′** in the lowest energy absorptions and the broaden of L_2L_1CT and ML_1CT absorption bands relative to the mononuclear **1**–**4** are induced by the much significant electronic delocalization imported by another Pt center and the more planar molecular structure. This result is consistent with the conclusions observed in torsional effects on nonplanar complexes (diphenylthiophene and 1,1′;4′,1″-terphenyl-4-thiol) [111,112]. Both the ML_1CT and L_2L_1CT transitions for **1**–**5** are affected in different media. Along with the increase of solvent polarity, the ML_1CT and L_2L_1CT transition are blue shifted. The distinction in **5** and **5′** is obvious, which is also resulted from the variation of the MO energy levels.

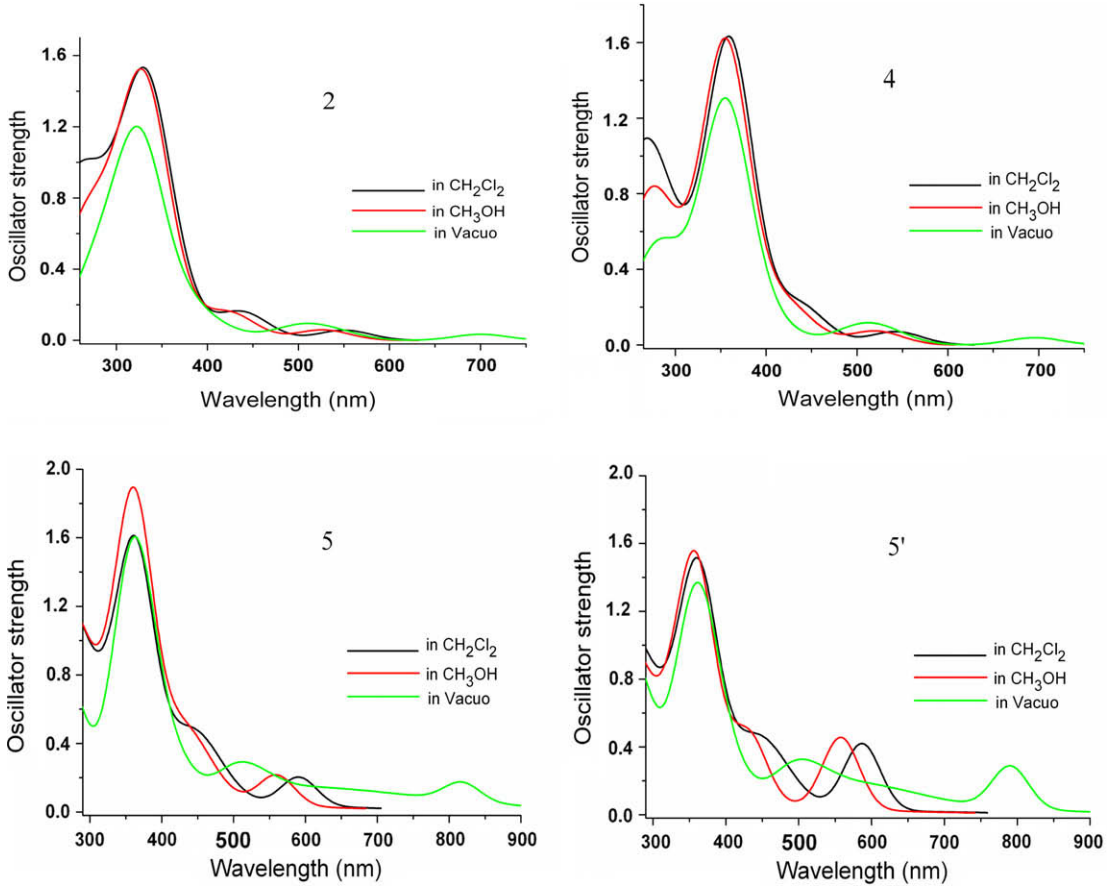

Fig. 10. Simulated absorption spectra of **2**, **4**, **5**, and **5′** in different surroundings.

Table 6
Phosphorescent emissions and ΔSCF energies of the complexes in CH_2Cl_2 solution with associated experimental values.

	Transition[a]		$\psi_v \rightarrow \psi_o$ (CI coefficient)	E_{ver},nm (eV)	Assignment	λ_{exptl} (nm)[b]	ΔSCF (nm/eV)
1	$^3A \rightarrow {}^1A$	L → H	120a → 119a (0.55)	615 (2.01)	L_1L_2CT/L_1MCT		559/2.22
		L+2 → H	122a → 119a (0.45)		π (L_2) → π(L_2)/L_1MCT		
2	$^3A \rightarrow {}^1A$	L → H	128a → 127a (0.55)	618 (2.01)	L_1L_2CT/L_1MCT	634	560/2.21
		L+2 → H	130a → 119a (0.45)		π (L_2) → π(L_2)/L_1MCT		
3	$^3A \rightarrow {}^1A$	L → H	136a → 135a (0.58)	621 (2.00)	L_1L_2CT/L_1MCT		566/2.19
		L+2 → H	138a → 135a (0.41)		π^*(L_2) → π(L_2)/L_1MCT		
4	$^3A \rightarrow {}^1A$	L+2 → H	128a → 125a (0.72)	607 (2.04)	π (L_2) → π(L_2)/L_2MCT	616	541/2.29
5	$^3B \rightarrow {}^1A$	L → H	97b → 98a (0.67)	671 (1.85)	L_1L_2CT/L_1MCT	651	683/1.81
5′	$^3A'' \rightarrow {}^1A'$	L → H	100a′ → 95a″ (0.70)	962 (1.29)	L_1L_2CT/L_1MCT		1000/1.24

[a] H denotes HOMO and L denotes LUMO.
[b] From Ref. [63], the experimental values of **4** and **5** are from the dimethyl derivatives of **4** and **5**, respectively.

Table 7
Calculated polarizabilities (α) and second-order polarizabilities (β_0) (or the static first hyperpolarizabilities).

	α (in the gas phase)	α (in CH_2Cl_2)	β_0 (in the gas phase)	β_0 (in CH_2Cl_2)
1	459	592	5733	4519
	(6.8×10^{-23} esu)	(8.8×10^{-23} esu)	(50×10^{-30} esu)	(39×10^{-30} esu)
2	480	598	5959	4980
	(7.1×10^{-23} esu)	(8.9×10^{-23} esu)	(52×10^{-30} esu)	(43×10^{-30} esu)
3	497	605	3334	2972
	(7.4×10^{-23} esu)	(9.0×10^{-23} esu)	(29×10^{-30} esu)	(26×10^{-30} esu)
4	506	647	4025	4270
	(7.5×10^{-23} esu)	(9.6×10^{-23} esu)	(35×10^{-30} esu)	(37×10^{-30} esu)
5	843	913	8546	8806
	(1.3×10^{-23} esu)	(13.5×10^{-23} esu)	(74×10^{-30} esu)	(76×10^{-30} esu)
5′	881	950	16655	17599
	(1.3×10^{-23} esu)	(14.1×10^{-23} esu)	(144×10^{-30} esu)	(152×10^{-30} esu)

The energies of phosphorescence from TD-DFT for **1**–**5** agree with the experimental data. However, there are some differences in the emission energies between the calculated from the ΔSCF method and the measured from experiments [113–117]. Based on our calculations, the emission wavelength of **5′** is out of the visible region. The emission characters are consistent between from TD-DFT method and the optimized triplet states. Except for **4**, the emissions of the complexes are just the reverse process of the lowest absorption, and the emissions can be attributed from the $^3L_1L_2CT/^3L_1MCT$ excited state. For **1**–**3**, the triplet excited state is combined a little of $^3[\pi^* \rightarrow \pi]$ character localized on the L_2 ligand. The emission transition of **4** is from LUMO+2 to HOMO and assigned as $^3[\pi^*(L_2) \rightarrow \pi\ (L_2)]/^3L_2MCT$. The absence of the $^3L_1L_2CT$ character in **4** is duo to its larger dihedral angle (θ) in triplet excited state than that in the ground state, the stronger electronic localization on the extended L_2 ligand, and the solvation effect.

3.4. NLO properties

Our calculations reveal the studied models possess acceptor–donor (A–D) and acceptor–donor–acceptor (A–D–A) configurations, and they should have distinct intramolecular charge transfer character under the external electronic field. We anticipate that these complexes offer some new interesting opportunities to nonlinear optical (NLO) materials [64,65]. The calculated polarizabilities (α) and the static first hyperpolarizabilities (β_0) of **1**–**5** are listed in Table 7.

With respect to **5** and **5′**, which have two electronic acceptor groups, their polarizabilities are about two times higher than **1**–**4**. The β_0 is termed the zero-frequency hyperpolarizability and is an estimate of the intrinsic molecular hyperpolarizability in the absence of any resonance effect. The β_0 values of these complexes are comparable to that of the most typical transition-metal compounds with extensive π-electron conjugation such ferrocenyl-terminated phenylethenyl oligomers, cyclopentadienyl (alkylphosphine) metal σ-acetylide complexes (M = Ru, Ni) (about 50–100×10^{-30} esu) [118–121]. From the "sum-over-states" (SOS) expression, Oudar and Chemla established a simple link between β_0 and a low-lying charge transfer transition by the two-level model [122,123]. For the static case (zero frequency), the β_0 is estimated from the formula $\beta_0 = (3/2)e^2\ \Delta\mu_{ge}(r_{ge}/E_{ge})^2$. The E_{ge}, r_{ge} and $\Delta\mu_{ge}$ are, respectively, the transition energy, the transition moment and the dipole moment variation, between the ground (g) and the involved excited (e) state. The oscillator strength is proportional to the transition energy and transition moment $f = (8\pi^2 m_e/3e^2h)E_{ge}r_{ge}^2$, thus, $\beta_0 \propto f\Delta\mu_{ge}(E_{ge})^{-3}$ [122–124]. The β_0 of **3** is about half of the analogues **1** and **2**, and the reason is that the f of **3** is decreased to 1/2 of that in **1** under similar transition energy and dipole moment variation. For **4**, the electronic donor reduces the electron-donating ability due to the enhancement of π-conjugation at the L_2 ligand, thus the β_0 of **4** is smaller than that of **1**. The static first hyperpolarizabilities of **5** are **5′**, especially **5′**, are enhanced compared to **1**–**4** since the considerably large f and smaller transition energy.

According to the above analysis, we can propose that, this kind of Pt acetylide complexes should be good candidate as the optoelectronic materials with large NLO response by altering the donors and/or acceptors and/or geometry of molecules, e.g., introducing electron-withdrawing substituent into the L_1 ligand, or decreasing the torsional angle between the donor and the acceptor planes.

4. Conclusion

We have performed a comprehensive study on the properties of the neutral substituted fluorene-based cyclometalated platinum(II)–acetylide complexes in the ground and excited states. The geometries of the complexes all show a nonplanar structure. The lowest energy absorption transitions exhibit LLCT/MLCT character since the electron-rich fluorene moieties possess the stronger

electron donating ability. The transition energies, EA and IP values are not impacted obviously by the dihedral angle between 60° and 75° in mononuclear complexes in **1**–**3**, but the oscillator strength of LLCT transition takes on a lower trend when the dihedral angle turn large. The oscillator strength is enhanced when the electrons are much delocalized for the dinuclear complex. The emission is assigned as the intraligand charge transfer when the electrons localize on the fluorene moieties in **4**. For the same reason, the $\pi - \pi^*$ (on the L_2 ligand) charge transfer transitions in the higher energy region decrease in energy when the fluorene is disubstituted by two ethynyls in **4**, **5**, and **5′**. These complexes can potentially act as the excellent NLO materials, owing to their large β_0 values and high transparencies. Lower transition energy with larger transition moment is the effective designing artifice on the new NLO material fields. Further studies on this aspect are in progress.

Acknowledgments

We thank the Natural Science Foundation of China (Grant Nos. 20573042 and 20333050) and the Research Fund for the Doctoral Program of Higher Education (Project No. 200801831004) for financial support of this work.

References

[1] R. Nast, Coord. Chem. Rev. 47 (1982) 89.
[2] P. Nguyen, P. Gomez-Elipe, I. Manners, Chem. Rev. 99 (1999) 1515.
[3] U.H.F. Bunz, Y. Rubin, Y. Tobe, Chem. Soc. Rev. 28 (1999) 107.
[4] C. Bruneau, P.H. Dixneuf, Acc. Chem. Res. 32 (1999) 311.
[5] I. Manners, Angew. Chem., Int. Ed. Engl. 35 (1996) 1602.
[6] P.F.H. Schwab, M.D. Levin, J. Michl, Chem. Rev. 99 (1999) 1869.
[7] T. Yamamoto, Bull. Chem. Soc. Jpn. 72 (1999) 621.
[8] D.L. Lichtenberger, S.K. Renshaw, A. Wong, C.D. Tagge, Organometallics 12 (1993) 3522.
[9] D.L. Lichtenberger, S.K. Renshaw, R.M. Bulluck, J. Am. Chem. Soc. 115 (1993) 3276.
[10] P.J. Kim, H. Masai, K. Sonogashira, N. Hagihara, Inorg. Nucl. Chem. Lett. 6 (1970) 181.
[11] N.J. Long, C.K. Williams, Angew. Chem., Int. Ed. 42 (2003) 2586.
[12] N.J. Long, Angew. Chem., Int. Ed. Engl. 34 (1995) 21.
[13] S. Barlow, D. O'Hare, Chem. Rev. 97 (1997) 637.
[14] M. Younus, A. Kohler, S. Cron, N. Chawdhury, M.R.A. Al-Madani, M.S. Khan, N.J. Long, R.H. Friend, P.R. Raithby, Angew. Chem., Int. Ed. 37 (1998) 3036.
[15] N. Chawdhury, A. Kohler, R.H. Friend, M. Younus, N.J. Long, P.R. Raithby, J. Lewis, Macromolecules 31 (1998) 722.
[16] V.W.W. Yam, K.K.W. Lo, K.M.C. Wong, J. Organomet. Chem. 578 (1999) 3.
[17] V.W.W. Yam, Acc. Chem. Res. 35 (2002) 555.
[18] M.J. Irwin, J.J. Vittal, R.J. Puddephatt, Organometallics 16 (1997) 3541.
[19] F. Paul, C. Lapinte, Coord. Chem. Rev. 178–180 (1998) 431.
[20] N. Tessler, G.J. Denton, R.H. Fried, Nature 382 (1996) 695.
[21] S.-C. Chan, M.C.W. Chan, Y. Wang, C.-M. Che, K.-K. Cheung, N. Zhu, Chem. Eur. J. 7 (2001) 4180.
[22] Y. Yang, D. Zhang, L.-Z. Wu, B. Chen, L.-P. Zhang, C.-H. Tung, J. Org. Chem. 69 (2004) 4788.
[23] D. Zhang, L.-Z. Wu, L. Zhou, X. Han, Q.-Z. Yang, L.-P. Zhang, C.-H. Tung, J. Am. Chem. Soc. 126 (2004) 3440.
[24] V.W.W. Yam, R.P.-L. Tang, K.M.C. Wong, K.K. Cheung, Organometallics 20 (2001) 4476.
[25] Z.J. Donhauser, B.A. Mantooth, K.F. Kelly, L.A. Bumm, J.D. Monnell, J.J. Stapleton Jr., D.W. Price, A.M. Rawlett, D.L. Allara, J.M. Tour, P.S. Weiss, Science 292 (2001) 2303.
[26] G.-J. Zhou, W.-Y. Wong, C. Ye, Z. Lin, Adv. Funct. Mater. 17 (2007) 963.
[27] C.W. Tang, S.A. Van Slyke, Appl. Phys. Lett. 51 (1987) 913.
[28] J. Lewis, M.S. Khan, A.K. Kakkar, B.F.G. Johnson, T.B. Marder, H.B. Fyfe, F. Wittmann, R.H. Friend, A.E. Dray, J. Organomet. Chem. 425 (1992) 165.
[29] G. Frapper, M. Kertesz, Inorg. Chem. 32 (1993) 732.
[30] K.A. Bunten, A.K. Kakkar, Macromolecules 29 (1996) 2885.
[31] N. Chawdhury, A. Köhler, R.H. Friend, W.Y. Wong, J. Lewis, M. Younus, P.R. Raithby, T.C. Corcoran, M.R.A. Al-Mandhary, M.S.J. Khan, Chem. Phys. 110 (1999) 4963.
[32] J.S. Wilson, A. Köhler, R.H. Friend, M.K. Al Suti, M.R.A. Al-Mandhary, M.S. Khan, P.R. Raithby, J. Chem. Phys. 113 (2000) 7627.
[33] W. Lu, B.-X. Mi, M.C.W. Chan, Z. Hui, C.-M. Che, N. Zhu, S.-T. Lee, J. Am. Chem. Soc. 126 (2004) 4958.
[34] R.C. Evans, P. Douglas, C.J. Winscom, Coord. Chem. Rev. 250 (2006) 2093.
[35] W.-Y. Wong, C.-L. Ho, Coord. Chem. Rev. 250 (2006) 2627.
[36] H. Masai, K. Sonogashira, N. Hagihara, Bull. Chem. Soc. Jpn. 44 (1971) 2226.
[37] K. Sonogashira, T. Yatake, Y. Tohda, S. Takahashi, N. Hagihara, J. Chem. Soc. Chem. Commun. (1977) 291.
[38] K. Sonogashira, N. Hagihara, S. Takahashi, Macromolecules 10 (1977) 879.
[39] K. Sonogashira, Y. Fujikura, T. Yatake, N. Toyoshima, S. Takahashi, N. Hagihara, J. Organomet. Chem. 145 (1978) 101.
[40] Y. Fujikura, K. Sonogashira, N. Hagihara, Chem. Lett. (1975) 1067.
[41] S. Takahashi, E. Murata, K. Sonogashira, N. Hagihara, J. Polym. Sci. Polym. Chem. Ed. 18 (1980) 661.
[42] C.W. Chan, L.K. Cheng, C.M. Che, Coord. Chem. Rev. 132 (1994) 87.
[43] J. Lewis, P.R. Raithby, W.-Y. Wong, J. Organomet. Chem. 556 (1998) 219.
[44] W.Y. Wong, K.H. Choi, G.L. Lu, J.X. Shi, Macromol. Rapid Commun. 22 (2001) 461.
[45] C. Wang, C. Yuan, H. Wu, Y.J. Wei, Appl. Lett. 78 (1995) 4264.
[46] X.-T. Tao, Y.-D. Zhang, T. Wada, H. Sasabe, H. Suzuki, T. Watanabe, S. Miyata, Adv. Mater. 10 (1998) 226.
[47] S. Maruyama, Y. Zhang, T. Wada, H. Sasabe, J. Chem. Soc., Perkin Trans. 1 (1999) 41.
[48] W.-Y. Wong, G.-L. Lu, K.-H. Choi, J.-X. Shi, Macromolecules 35 (2002) 3506.
[49] R. Ziessel, M. Hissler, A. El-ghayoury, A. Harriman, Coord. Chem. Rev. 178–180 (1998) 1251.
[50] M. Hissler, J.E. McGarrah, W.B. Connick, D.K. Geiger, S.D. Cummings, R. Eisenberg, Coord. Chem. Rev. 208 (2000) 115.
[51] D.R. McMillin, J.J. Moore, Coord. Chem. Rev. 229 (2002) 113.
[52] F.N. Castellano, I.E. Pomestchenko, E. Shikhova, F. Hua, M.L. Muro, N. Rajapakse, Coord. Chem. Rev. 250 (2006) 1819.
[53] J.A. Gereth Williams, Top. Curr. Chem. 281 (2007) 205.
[54] S.W. Lai, M.C.W. Chan, K.K. Cheung, C.M. Che, Organometallics 18 (1999) 3327.
[55] S.W. Lai, M.C.W. Chan, T.C. Cheung, S.M. Peng, C.M. Che, Inorg. Chem. 38 (1999) 4046.
[56] F. Neve, M. Ghedini, A. Crispini, J. Chem. Soc., Chem. Commun. (1996) 2463.
[57] T.C. Cheung, K.K. Cheung, S.M. Peng, C.M. Che, J. Chem. Soc., Dalton Trans. (1996) 1645.
[58] C.W. Chan, T.F. Lai, C.M. Che, S.M. Peng, J. Am. Chem. Soc. 115 (1993) 11245.
[59] W. Lu, M.C.W. Chan, K.K. Cheung, C.M. Che, Organometallics 20 (2001) 2477.
[60] V.W.W. Yam, R.P.L. Tang, K.M.C. Wong, C.C. Ko, K.K. Cheung, Inorg. Chem. 40 (2001) 571.
[61] J.F. Michalec, S.A. Bejune, D.R. McMillin, Inorg. Chem. 39 (2000) 2708.
[62] G. Arena, G. Calogero, S. Campagna, L.M. Scolaro, V. Ricevuto, R. Romeo, Inorg. Chem. 37 (1998) 2763.
[63] J.B. Seneclauze, P. Retailleau, R. Ziessel, New J. Chem. 31 (2007) 1412.
[64] S.D. Bella, Chem. Soc. Rev. 30 (2001) 355. and references therein.
[65] C.E. Powell, M.G. Humphrey, Coord. Chem. Rev. 248 (2004) 725. and references therein.
[66] X. Zhou, Q.-J. Pan, B.-H. Xia, M.-X. Li, H.-X. Zhang, A.-C. Tung, J. Phys. Chem. A 111 (2007) 5465.
[67] X.-J. Liu, J.-K. Feng, J. Meng, Q.-J. Pan, A.-M. Ren, X. Zhou, H.-X. Zhang, Eur. J. Inorg. Chem. (2005) 1856.
[68] T. Cardolaccia, Y. Li, K.S. Schanze, J. Am. Chem. Soc. 130 (2008) 2535.
[69] J.C. Amicangelo, J. Chem. Theory Comput. 3 (2007) 2198.
[70] S.R. Stoyanov, J.M. Villegas, D.P. Rillema, Inorg. Chem. 42 (2003) 7852.
[71] L.-L. Shi, Y. Liao, G.-C. Yang, Z.-M. Su, S.-S. Zhao, Inorg. Chem. 47 (2008) 2347.
[72] W. Koch, M.C. Holthausen, A Chemist's Guide to Density Functional, Theory, Wiley-VCH, Weinheim, Germany, 2000.
[73] C. Adamo, B.V. di Matteo, Adv. Quantum Chem. 36 (1999) 4.
[74] E. Runge, E.K.U. Gross, Phys. Rev. Lett. 52 (1984) 997.
[75] C. Lee, W. Yang, R.G. Parr, Phys. Rev. B 37 (1988) 785.
[76] A.D. Becke, J. Chem. Phys. 98 (1993) 5648.
[77] K. Nozaki, K. Takamori, Y. Nakatsugawa, T. Ohno, Inorg. Chem. 45 (2006) 6161.
[78] B. Miehlich, A. Savin, H. Stoll, H. Preuss, Chem. Phys. Lett. 157 (1989) 200.
[79] P.J. Hay, W.R. Wadt, J. Chem. Phys. 82 (1985) 270.
[80] W.R. Wadt, P.J. Hay, J. Chem. Phys. 82 (1985) 284.
[81] P.J. Hay, W.R. Wadt, J. Chem. Phys. 82 (1985) 299.
[82] P.C. Hariharan, J.A. Pople, Mol. Phys. 27 (1974) 209.
[83] E. Glimsdal, M. Carlsson, B. Eliasson, B. Minaev, M. Lindgren, J. Phys. Chem. A 111 (2007) 244.
[84] T.M. Cooper, D.M. Krein, A.R. Burke, D.G. McLean, J.E. Rogers, J.E. Slagle, J. Phys. Chem. A 110 (2006) 13370.
[85] Z. He, W.-Y. Wong, X. Yu, H.-S. Kwok, Z. Lin, Inorg. Chem. 45 (2006) 10922.
[86] B. Hirani, J. Li, P.I. Djurovich, M. Yousufuddin, J. Oxgaard, P. Persson, S.R. Wilson, R. Bau, W.A. Goddard III, M.E. Thompson, Inorg. Chem. 46 (2007) 3865.
[87] W. Sotoyama, T. Satoh, H. Sato, A. Matsuura, N. Sawatari, J. Phys. Chem. A 109 (2005) 9760.
[88] C. Jamorski, M.E. Casida, D.R. Salahub, J. Chem. Phys. 104 (1996) 5134.
[89] M. Petersilka, U.J. Grossmann, E.K.U. Gross, Phys. Rev. Lett. 76 (1996) 1212.
[90] R. Bauernschmitt, R. Ahlrichs, F.H. Hennrich, M.M. Kappes, J. Am. Chem. Soc. 120 (1998) 5052.
[91] M.E. Casida, C. Jamorski, K.C. Casida, D.R. Salahub, J. Chem. Phys. 108 (1998) 4439.
[92] R.E. Stratmann, G.E. Scuseria, M.J. Frisch, J. Chem. Phys. 109 (1998) 8218.
[93] W. Chen, Z.R. Li, D. Wu, Y. Li, C.C. Sun, J. Phys. Chem. A 109 (2005) 2920.
[94] M. Cossi, G. Scalmani, N. Regar, V. Barone, J. Chem. Phys. 117 (2002) 43.
[95] V. Barone, M. Cossi, J. Tomasi, J. Chem. Phys. 107 (1997) 3210.

[96] D. Andrae, U. Haussermann, M. Dolg, H. Stoll, H. Preuss, Theor. Chim. Acta 77 (1990) 123.
[97] M. Dolg, P. Pyykkö, N. Runeberg, Inorg. Chem. 35 (1996) 7450.
[98] M.J. Frisch, G.W. Trucks, H.B. Schlegel, G.E. Scuseria, M.A. Robb, J.R. Cheeseman, J.A. Montgomery Jr., T. Vreven, K.N. Kudin, J.C. Burant, J.M. Millam, S.S. Iyengar, J. Tomasi, V. Barone, B. Mennucci, M. Cossi, G. Scalmani, N. Rega, G.A. Petersson, H. Nakatsuji, M. Hada, M. Ehara, K. Toyota, R. Fukuda, J. Hasegawa, M. Ishida, T. Nakajima, Y. Honda, O. Kitao, H. Nakai, M. Klene, X. Li, J.E. Knox, H.P. Hratchian, J.B. Cross, V. Bakken, C. Adamo, J. Jaramillo, R. Gomperts, R.E. Stratmann, O. Yazyev, A.J. Austin, R. Cammi, C. Pomelli, J.W. Ochterski, P.Y. Ayala, K. Morokuma, G.A. Voth, P. Salvador, J.J. Dannenberg, V.G. Zakrzewski, S. Dapprich, A.D. Daniels, M.C. Strain, O. Farkas, D.K. Malick, A.D. Rabuck, K. Raghavachari, J.B. Foresman, J.V. Ortiz, Q. Cui, A.G. Baboul, S. Clifford, I. Komaromi, R.L. Martin, D.J. Fox, T. Keith, M.A. Al-Laham, C.Y. Peng, A. Nanayakkara, M. Challacombe, P. M.W. Gill, B.Johnson, W. Chen, M.W. Wong, C. Gonzalez, J.A. Pople, GAUSSIAN 03, revision C.02, Gaussian Inc., Wallingford, CT, 2004.
[99] M. Oda, H.-G. Nothofer, U. Scherf, V. Šunjić, D. Richter, W. Regenstein, D. Neher, Macromolecules 35 (2002) 6792.
[100] J.-F. Wang, J.-K. Feng, A.-M. Ren, X.-J. Liu, Y.-G. Ma, P. Lu, H.-X. Zhang, Macromolecules 37 (2004) 3451.
[101] S. Fantacci, F. De Angelis, A. Selloni, J. Am. Chem. Soc. 125 (2003) 4381.
[102] M.-F. Charlot, Y. Pellegrin, A. Quaranta, W. Leibl, A. Aukauloo, Chen. Eur. J. 12 (2006) 796.
[103] M.-F. Charlot, A. Aukauloo, J. Phys. Chem. A 111 (2007) 11661.
[104] A. Rosa, G. Ricciardi, O. Gritsenko, E. Baerends, J. Struct. Bond. 112 (2004) 49.
[105] S.J.A. Gisbergen, J.A. Groeneveld, A. Rosa, J.G. Snijders, E.J. Baerends, J. Phys. Chem. A 103 (1999) 6835.
[106] A. Vlček, S. Zališ, Coord. Chem. Rev. 251 (2007) 258.
[107] M.E. Casida, F. Gutierrez, J. Guan, F.X. Gadea, D. Salahub, J.P. Daudey, J. Chem. Phys. 113 (2000) 7062.
[108] Z.L. Cai, K. Sendt, J.R. Reimers, J. Chem. Phys. 117 (2002) 5543.
[109] A. Dreuw, J.L. Weisman, M. Head-Gordon, J. Chem. Phys. 119 (2003) 2943.
[110] S. Grimme, M. Parac, ChemPhysChem 3 (2003) 292.
[111] M. Piacenza, F. Della Sala, E. Fabiano, T. Maiolo, G. Gigli, J. Comput. Chem. 29 (2008) 451.
[112] C. Grave, C. Risko, A. Shaporenko, Y. Wang, C. Nuckolls, M.A. Ratner, M.A. Rampi, M. Zharnikov, Adv. Funct. Mater. 17 (2007) 3816.
[113] I. Avilov, P. Marsal, J.L. Brédas, D. Beljonne, Adv. Mater. 16 (2004) 1624.
[114] I. Avilov, P. Minoofar, J. Cornil, L.D. Cola, J. Am. Chem. Soc. 129 (2007) 8247.
[115] D.A. Dos Santos, D. Beljonne, J. Cornil, J.L. Brédas, Chem. Phys. 227 (1998) 1.
[116] D. Beljonne, J. Cornil, J.L. Brédas, R.H. Friend, R.A.J. Janssen, J. Am. Chem. Soc. 118 (1996) 6453.
[117] D. Beljonne, H.F. Wittmann, A. Köhler, S. Graham, M. Younus, J. Lewis, P.R. Raithby, M.S. Khan, R.H. Friend, J.L. Brédas, J. Chem. Phys. 105 (1996) 3868.
[118] I.R. Whittall, A.M. McDonagh, M.G. Humphrey, M. Samoc, Adv. Organomet. Chem. 42 (1998) 291.
[119] B.J. Coe, Chem. Eur. J. 5 (1999) 2464.
[120] B.J. Coe, J.A. Harris, I. Asselberghs, A. Persoons, J.C. Jeffery, L.H. Rees, T. Gelbrich, M.B. Hursthouse, J. Chem. Soc., Dalton Trans. (1999) 3617.
[121] B.J. Coe, J.A. Harris, K. Clays, A. Persoons, K. Wostyn, B.S. Brunschwig, Chem. Commun. (2001) 1548.
[122] J.L. Oudar, D.S. Chemla, J. Chem. Phys. 66 (1977) 2664.
[123] J.L. Oudar, J. Chem. Phys. 67 (1977) 446.
[124] D.R. Kanis, M.A. Ratner, T.J. Marks, Chem. Rev. 94 (1994) 195.